Ionic liquid ultrathin films at the surface of Cu(100) and Au(111)

Aleksandra B. Biedron,[1] Eric L. Garfunkel,[1] Edward W. Castner Jr.,[1] and Sylvie Rangan[2]
[1]*Department of Chemistry and Chemical Biology, Rutgers University, 610 Taylor Road, Piscataway, New Jersey 08854, USA*
[2]*Department of Physics and Astronomy and Laboratory for Surface Modification, Rutgers University, 136 Frelinghuysen Road, Piscataway, New Jersey 08854, USA*

(Received 12 September 2016; accepted 17 January 2017; published online 6 February 2017)

Monolayer to multilayer ultrathin films of the ionic liquid (IL) 1-methyl-3-octylimidazolium bis(trifluoromethylsulfonyl)amide have been prepared on Au(111) and Cu(100) surfaces using physical vapor deposition. The ion-surface interactions are studied using a combination of scanning tunnel microscopy, as well as ultraviolet and x-ray photoemission spectroscopies. It is found that the IL does not decompose at the surface of the metals, and that the IL interaction with the Cu(100) surface is much stronger than with the Au(111) surface. As a consequence, STM imaging at room temperature results in more stable imaging at the monolayer coverage on Cu(100) than on Au(111), and work function measurements indicate a large interface dipole upon deposition of a monolayer of IL on Cu. Additional IL depositions on the two surfaces result in two distinct behaviors for the IL core levels: a gradual energy shift of the core levels on Au and a set of two well defined monolayer and multilayer core level components found at fixed energies on Cu, due to the formation of a tightly bound monolayer. Finally, it is proposed that the particularly strong cation-Cu interaction leads to stabilization of the anion and prevents its decomposition at the surface of Cu(100). *Published by AIP Publishing.* [http://dx.doi.org/10.1063/1.4975101]

I. INTRODUCTION

Research into ionic liquids (ILs) for energy and materials applications continues to expand, since these intrinsic electrolytes offer a number of advantages for battery and supercapacitor technologies.[1] A conventional synthetic route for making ionic liquids involves preparation of the anionic and cationic components separately, followed by an ion exchange step. This permits straightforward customization of both the IL anions and cations for specific tasks.[2] It is common for either the IL anion or cation to be strongly amphiphilic, as a result of local charge density combined with the presence of a hydrophobic tail such as an alkyl chain. Such properties can lead to a high degree of ordering in the bulk structure of the ILs.[3] Additionally, the structural correlations in the bulk ILs are often found to be quite different from those at the IL-metal[4,5] or IL-vacuum interfaces.[6] Understanding, controlling, and ultimately designing the structural features of ILs at interfaces will be key to enhancing their performance, especially for applications to electrical double-layer capacitors, batteries, and nanoscale tribology. For example, knowledge of ionic behavior at a surface can be crucial for developing optimized electrolyte-electrode combinations in real life energy devices, and necessitates probing IL-metal interfaces at the Ångstrom level that are often obscured by a μm-thick IL layer. Reports on the IL organization within the bulk and at the gas-liquid interface are becoming more common,[3,6–18] however, insights into this hidden interface have been more limited and often necessitate a surface science approach, using atomic force microscopy,[4,5,19] x-ray photoemission spectroscopy (XPS),[20–27] UV-photoemission spectroscopy (UPS),[27–35] inverse photoemission spectroscopy (IPS),[30] helium atom scattering,[36] or scanning tunneling microscopy (STM).[34,37–40]

The intrinsically low vapor pressure of most ionic liquids enables their use for controlled deposition of ultrathin films using physical vapor deposition (PVD) in ultrahigh vacuum (UHV).[23,24,41] When such films are prepared on atomically flat surfaces, the specific interactions between the constituent anions and cations of the IL and the supporting surface can be probed using a range of surface science techniques. Here, we have chosen to study the interface of 1-octyl-3-methylimidazolium bis(trifluoromethanesulfonyl) amide ($Im^+_{8,1}/NTf^-_2$, shown in Fig. 1), an electrochemically and thermodynamically stable IL compatible with UHV applications,[21,23,39] with two metal surfaces, Au(111) and Cu(100). Information about the $Im^+_{8,1}/NTf^-_2$-Au(111) interface is available from previous angle-resolved XPS studies.[23,24] In particular, Cremer *et al.* have observed continuous-monolayer adsorption of this IL onto Au(111) without decomposition, and proposed that each ion would form a checkerboard pattern at the monolayer level so as to minimize repulsive forces.[23] Using our experimental setup, we can thus compare the weak adsorption of $Im^+_{8,1}/NTf^-_2$ on Au(111), as a reference, to its potentially stronger interaction with Cu(100). Indeed, on Cu(111), decomposition of NTf^-_2 paired with 1-butyl-1-methylpyrrolidinium has been previously reported by Uhl *et al.*[38]

In this work, we have used a combination of STM, XPS, and UPS, in order to obtain a global picture of the IL morphology and electronic structure from the monolayer to the multilayer regime, by sequential deposition of $Im^+_{8,1}/NTf^-_2$ on the clean Au(111) and Cu(100) surfaces using PVD. STM provides monolayer-thick coverage morphology. Information

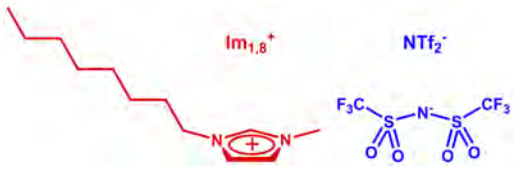

FIG. 1. Chemical structures of the 1-methyl-3-octylimid-azolium cation (left) and bis(trifluoromethanesulfonyl)amide anion (right).

on the chemical environment is obtained from valence band (VB) and core levels, while measurement of the work function (WF) characterizes the formation of interface dipoles at the IL/surface interface.

II. METHODS

A. Photoelectron spectroscopy

The photoelectron spectroscopy experiments presented here were measured using a Thermo Scientific ESCALAB 250xi instrument. XPS measurements used a monochromated Al Kα line with photon energy of 1486.7 eV and an energy resolution of about 0.6 eV. The measurements were performed in a geometry where the measured photoelectrons are collected in normal emergence. The estimated depth sensitivity in this geometry is about 10 nm. UPS measurements were made using the He IIα line (40.8 eV) of a He plasma source, with a resolution better than 0.1 eV. Secondary electron cutoff (SECO) spectra were measured on biased samples using the He I line (21.2 eV) to measure the work function, given by $WF = h\nu - W$, where $h\nu$ is the photon source energy and W the total width of the emitted photoelectrons. The parasitic He IIβ line has been subtracted to obtain the valence band (VB) spectra presented in this work. As noted in prior work, significant changes in photoemission spectra from beam damage were not observed within our limited acquisition time.[42] The binding energy in UPS was referenced to the metal Fermi level, with Ef = 0; binding energies of occupied states are listed as negative energies. The XPS binding energies were referenced to the Au $4f_{7/2}$ and Cu $2p_{3/2}$ peak positions measured at −84.0 eV and −932.6 eV, respectively. UPS spectra are compared with densities of states (DOS) obtained from standard electronic structure calculations on the gas phase discrete anion, cation, and ion pair using the GAMESS program suite.[43]

B. Scanning tunneling microscopy methods

STM measurements were performed in a UHV environment at pressures below 5×10^{-10} Torr with an Omicron STM instrument. The STM tip was electrochemically etched from a 0.25 mm diameter tungsten wire. The images presented here were obtained in constant-current mode with the sample at room temperature. Images were processed using the WSxM software.[44] Uncertainties in the STM images are conservatively estimated to be ±0.1 Å for vertical distances, ±1 Å for lateral distances, and ∼3° for angles; these uncertainties arise from a combination of ambient noise and drift during imaging. Surface coverage was estimated from XPS results obtained in the same UHV system.

C. Sample preparation

A clean and atomically flat Au(111) surface [Agilent Technologies, 150 nm Au on mica] was obtained by performing cycles of argon ion sputtering (0.5 kV) and annealing (400 °C). The clean Cu(100) surface was prepared from a single crystal with repeated cycles of argon ion sputtering (2 kV) and annealing (500 °C).

The $Im_{1,8}^+/NTf_2^-$ ionic liquid (≥99% purity) was purchased from IoLiTec (Ionic Liquid Technologies, Inc., Tuscaloosa AL). The IL, depicted in Fig. 1, was deposited by physical vapor deposition in UHV using a Knudsen cell with the temperature set in a range between 150 and 230 °C. The IL sample was thoroughly degassed prior to deposition. Mass spectrometry of the vapor of this IL has been reported and indicates a predominance of anion-cation pairs.[45–49]

In this work, a monolayer coverage is defined by the convergence of two observations: (1) When a surface covered with a thick multilayer is annealed at 130 °C for 10 min, the weakly bound IL components are desorbing and leave a layer at the surface, with a stoichiometry and chemical environment corresponding to the intact IL. This monolayer preparation technique is often referred to as the top-down approach for organic thin films. (2) The coverage thus obtained also coincides with the maximum coverage on the Cu(100) surface with an IL layer in close proximity to the surface. The corresponding experimental data will be introduced later in the text. The number of layers has been estimated assuming a constant evaporation rate for each deposition.

Alternatively, the thickness of the IL films can be estimated using the attenuation of the photoemission signals from the metal substrates with increasing numbers of adlayers, since it was reported that the IL growth on Au(111) occurred layer by layer at least up to 2 to 3 MLs.[23] The attenuation lengths for the relevant electrons ejected from the metal into the IL layer have been calculated using the NIST electron effective attenuation length database software.[50] For our experimental geometry using the Al-Kα X-ray source and an IL density of 1.32 g cm^{-3}, the calculated attenuation lengths for the photoemitted electrons inside the IL layer are 19.8 Å for Cu 2p, 42.8 Å for Au 4f, and 37.6 Å for C 1s. The thicknesses calculated from photoemission for 1 ML on Au(111) and Cu(100) were 7.5Å in average, consistent with the value reported for one molecular layer.[23,24]

III. RESULTS AND DISCUSSION

A. Surface morphology and adsorption strength of IL films via STM

To explore the morphology of the $Im_{1,8}^+/NTf_2^-$ films on the Au(111) and Cu(100) surfaces, STM measurements were performed at room temperature before and after deposition of one monolayer of the IL. The STM images are shown in Fig. 2.

The STM image of the clean Au(111) surface is shown in Fig. 2(a) and possesses the characteristic herringbone pattern of the clean Au(111) with well-defined soliton walls. After deposition of the IL on the clean Au(111) surface, similar soliton walls were observed, as shown in Fig. 2(b) and in the inset

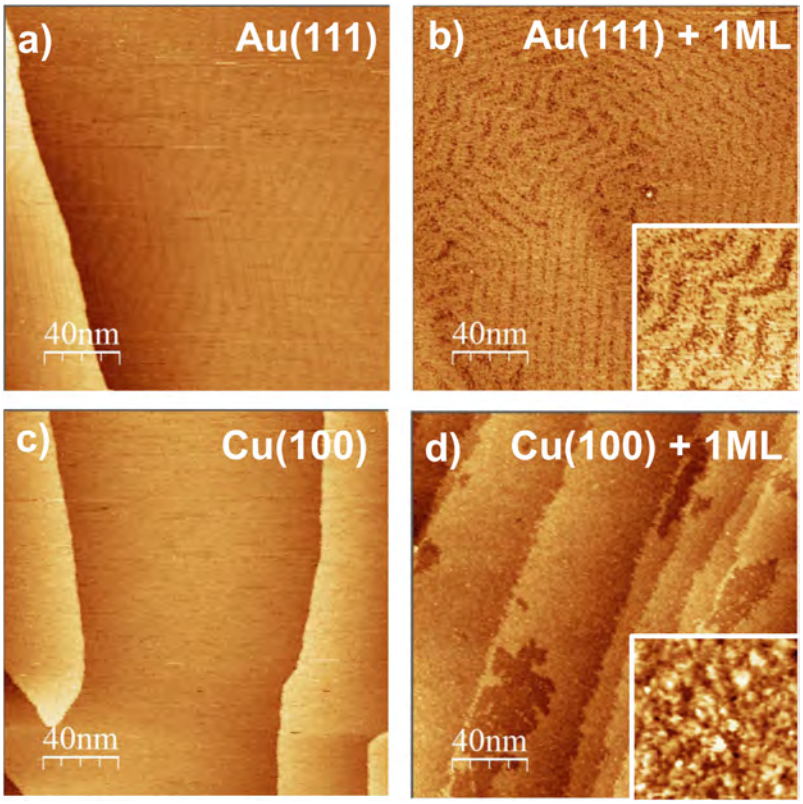

FIG. 2. STM images obtained on the Au(111) and Cu(100) surfaces, before ((a) and (c), respectively) and after deposition of a monolayer of the $Im^{+}_{8,1}/NTf^{-}_{2}$ IL ((b) and (d), respectively). Insets show a 40×40 nm^2 area of the corresponding surfaces.

of Fig. 2(b). However, the surface appeared streaky, indicating either the presence of mobile IL species and/or species interacting with the STM tip, as reported previously.[39] The Au surface did not appear to be affected by the presence of the IL: no alteration of the step edges morphology or of the characteristics of the soliton walls was visible.

The STM image of clean Cu(100) is shown in Fig. 2(c) and is smooth and featureless. The STM image of one ML of the IL on the Cu(100) surface is shown in Fig. 2(d). Contrary to what was observed on the Au(111) surface, there is no evidence for mobile surface species, indicating a stronger IL-surface interaction, capable of preventing diffusion of the IL adsorbates even at room temperature. In particular, the inset of Fig. 2(d) indicates the presence of a stable surface without large scale streakiness but indicating no clear order of the adsorbate. This may be understood by assuming that only parts of the IL are strongly bound to the surface (such as the cationic imidazolium ring) leaving mobile parts (such as the alkyl tail) able to reorient. Additionally, open structures were observed after deposition of about 1 ML, with a depth of about 1.5 Å, which could be attributed either to a hole in the IL monolayer or to a Cu step edge height.

The absence of local order at room temperature for IL species on surfaces has been previously reported and only low temperature imaging was able to resolve molecular ordering of the adlayer. These results are consistent with previous observations of $Im^{+}_{1,8}/NTf^{-}_{2}$ on Au(111) by Uhl *et al.*, where 2D island growth was reported at 77 K, that melted below 200 K.[39] In our case, STM measurements indicate that the IL-surface interaction strength is far greater on the Cu(100). For any information related to the chemical species present at the surface and the nature of the IL-surface bond, additional spectroscopic measurements are necessary.

B. Electronic structure of the IL

In order to explore the IL-surface interactions, it is useful to consider the electronic structure of the IL anions and cations obtained from both UPS and XPS. To this end, thick multilayers can be grown and analyzed, for which the influence of the substrate becomes negligible. At the top of Fig. 3 the VB spectrum measured for such a multilayer using UPS is shown in black. Below the experimental spectrum, the DOS spectrum calculated for the IL anion and cation pair (shown in Fig. S1 of the supplementary material) is shown in green, with

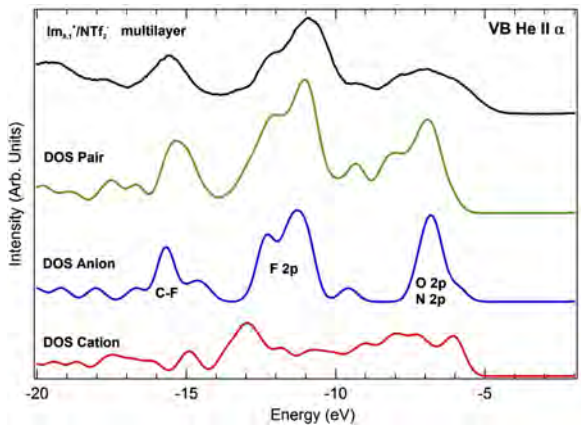

FIG. 3. VB spectra measured on a thick film of $Im^{+}_{8,1}/NTf^{-}_{2}$ deposited in UHV on gold. The DOSs calculated for the ion pair and for individual ions are also shown, shifted in energy so as to match experimental features.

the anionic and cationic DOS shown in blue and red, respectively. The calculated spectra are rigidly shifted in energy to align the DOS with the features of the experimental spectrum.

The results obtained here are compatible with previous reports of VB spectra for dialkylimidazolium NTf_2^- ILs.[28–31,33,35] As a result of the intrinsic breadth of the cationic contributions to the VB spectrum, the experimental VB spectrum resembles the DOS calculated for the anion. Moreover, atomic photoemission cross sections effectively decrease the cation contribution, as the C 2p cross section is smaller than the cross section of the O 2p or F 2p levels, as illustrated in Fig. S2 of the supplementary material. Thus, the VB spectra measured using UPS reflect mostly the contributions from the anion. This allows us to assign the states measured between −6 eV and −8 eV to O 2p and N 2p hybridized states, the ones found between −10 eV and −13 eV to primarily F 2p hybridized states, and features near −15 eV to C–F bonds on the NTf_2^- anion.

Core levels pertaining to the IL pair, C 1s, N 1s, F 1s, O 1s, and S 2p, have been measured using XPS on the thick multilayer. Two core levels useful for our interface study, C 1s and N 1s, are shown in Figs. 4(a) and 4(b), respectively, with their decomposition and attribution. The correct stoichiometry is obtained considering the C 1s and N 1s XPS spectra shown in Figs. 4(a) and 4(b), respectively. Fits to the C 1s spectra show that seven of the alkyl tail carbon atoms give rise to the peak at −285.0 eV, with the three imidazolium ring carbon atoms and two N-methyl carbon atoms leading to the broader peak at −286.9 eV in Fig. 4(a), while the anionic trifluoromethyl carbon peak is observed at −292.9 eV. The N 1s spectrum of Fig. 4(b) shows the anion contribution at −399.5 eV, while the signal from the two imidazolium ring nitrogens is observed at −402.2 eV. The remaining core levels, each originating from a single chemical environment, are straightforward to interpret and are available in Fig. S3 of the supplementary material. We note that the measured chemical composition is in good agreement with the expected molecular formula as shown in Table S2 of the supplementary material. These results are comparable to earlier work on similar ILs.[20,21,23–26]

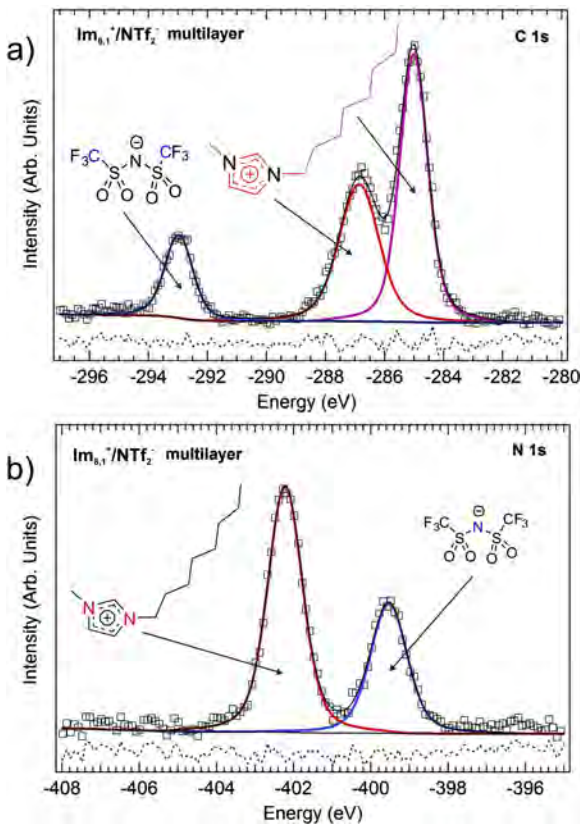

FIG. 4. C 1s and N 1s core levels measured on a thick film of $Im_{8,1}^+/NTf_2^-$ deposited in UHV on gold. The deconvolution of the core levels and their attribution is indicated. The dotted line indicates the fit residue.

C. Interfacial electronic structure

In order to explore the interfacial properties of the IL on the two Au(111) and Cu(100) surfaces, UPS and XPS measurements were performed on each surface before and after sequential depositions of the IL. The resulting VB and secondary electron cutoff (SECO) spectra are shown in Figs. 5(a) and 5(b), respectively, for the Au(111) surface and in Figs. 5(c) and 5(d), respectively, for the Cu(100) surface. Core levels acquired on the same surfaces are shown in Fig. 6, for the Au(111) and Cu(100) surfaces.

The VB spectrum of the initially prepared surface, shown in Fig. 5(b), is characteristic of clean Au(111). A WF of 4.9 eV is measured from the SECO of Fig. 5(a), in good agreement with previous work.[51] After deposition of ∼1 ML of the IL, the VB spectrum now presents additional features that can be related to IL states. Above −8 eV, the Au contribution to the spectrum is too large to directly discern the states of the IL monolayer. However, below this energy, F 2p states and C–F p-bond related states are clearly visible centered at −9.7 eV (for the largest peak) and −14.5 eV, respectively. Upon IL deposition, the WF at the surface decreases by less than 0.2 eV.

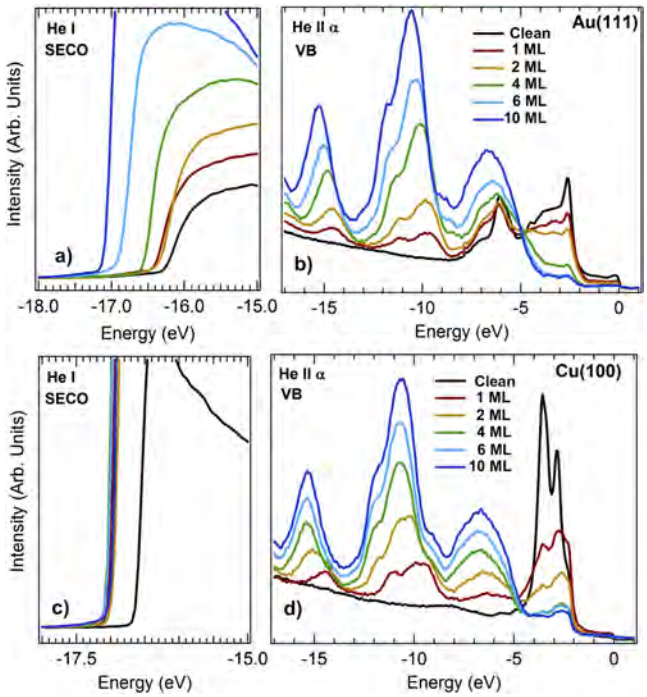

FIG. 5. UPS spectra of SECO and VB measured on the Au(111) ((a) and (b), respectively) and Cu(100) ((c) and (d), respectively) surfaces before and after sequential IL deposition.

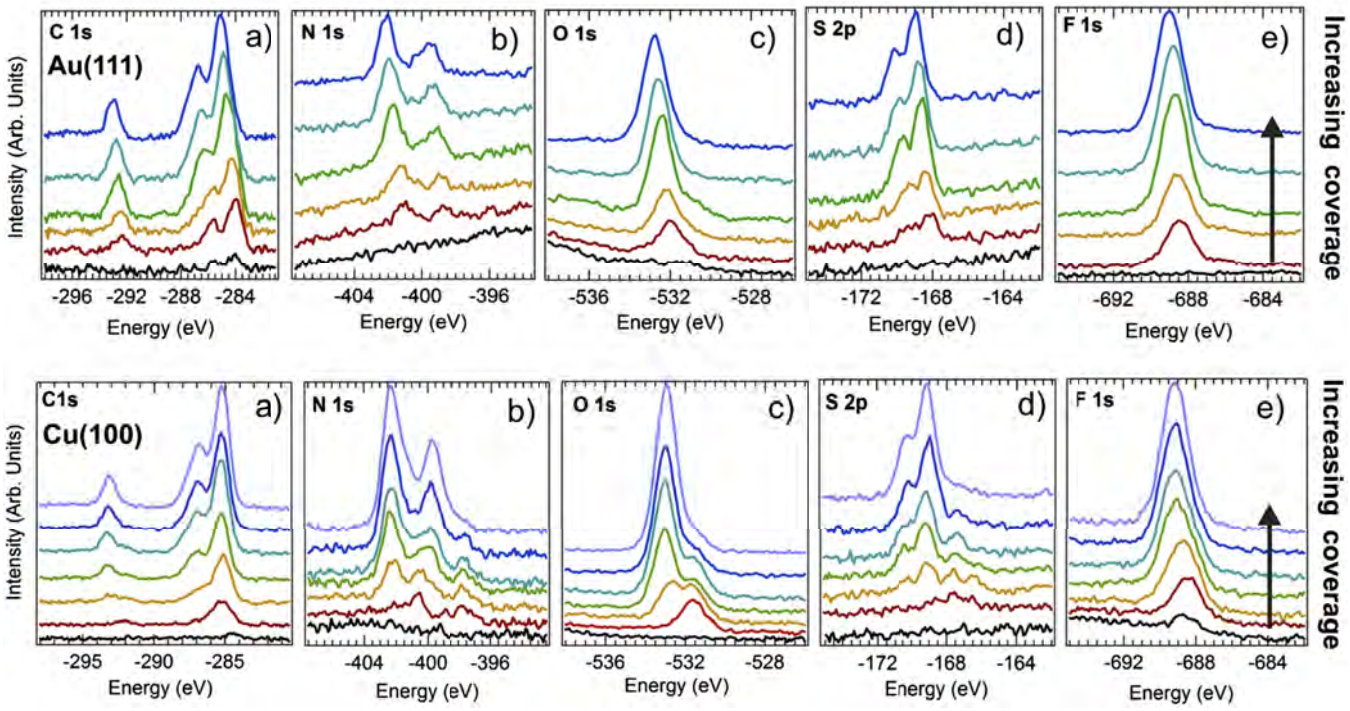

FIG. 6. XPS core levels for C 1s, N 1s, O 1s, S 2p, and F 1s, measured for clean surfaces and following subsequent deposition of the IL. Top: Au(111) surface; bottom: Cu(100) surface. Coverages are similar to the one of Fig. 5.

Additional sequential depositions of the IL slowly increase the contribution from the IL. For 10 ML of IL coverage, most of the Au(111) surface contribution is suppressed. During this gradual film growth, the molecular peaks progressively shift to higher binding energies with an average of 0.2 eV per deposition cycle. Concomitantly, the surface WF gradually decreases by 0.2 eV in average, to achieve the final value of 3.9 eV.

In the case of the Cu(100) surface, characteristic Cu 3d states are visible in the VB of the clean surface shown in Fig. 5(d), just below the Fermi edge, and a WF of 4.5 eV is obtained from the SECO of Fig. 5(c) in good agreement with previous work.[52] Upon deposition of about 1 ML of IL, F 2p and C–F p states are observed centered at −9.6 (for the highest peak) eV and −14.4 eV, respectively, similar to what was observed on the Au(111) surface. However, the behavior of the surface WF is drastically different: a strong decrease of 0.5 eV is measured for 1 ML coverage. At about 2 ML coverage, the C–F related states and F 2p related states appear broader, due to the overlap of two different contributions: one is similar to that measured for 1 ML coverage and the other having a similar appearance but shifted toward higher binding energies. Deposition of additional IL monolayers increases the latter contribution at fixed energies: the C–F states are now found centered at −15.3 eV, while the highest peak of the F 2p states is found at −10.7 eV. It is also observed that to within experimental uncertainties, the Cu WF does not further decrease on deposition of additional MLs of IL.

It is useful to qualitatively compare the UPS results to the XPS measurements of the same sequentially grown films of IL. The core levels associated with the IL and measured on Au(111) are presented in the top part of Fig. 6, as a function of increasing coverage, and are found consistent with previous reports.[23,25] At first glance, the shape of the individual core levels is not altered from one deposition to another, but the core levels seem to simply shift rigidly by an average of 0.2 eV toward higher binding energies following each deposition step. These numbers are comparable in magnitude and direction to the shifts observed for the surface vacuum level as well as for the VB states of the IL deposited on the same surface. Fits to the N 1s and C 1s XP spectra for a deposition of 4 ML of IL on Au(111) are shown in Figs. 7(a) and 7(b), respectively. The analysis method for these core levels is similar to the one used for the thick multilayer. Parameters for these core levels and the analysis of the remaining S 2p, O 1s, and F 1s core level for the same coverage can be found in Fig. S4 of the supplementary material.

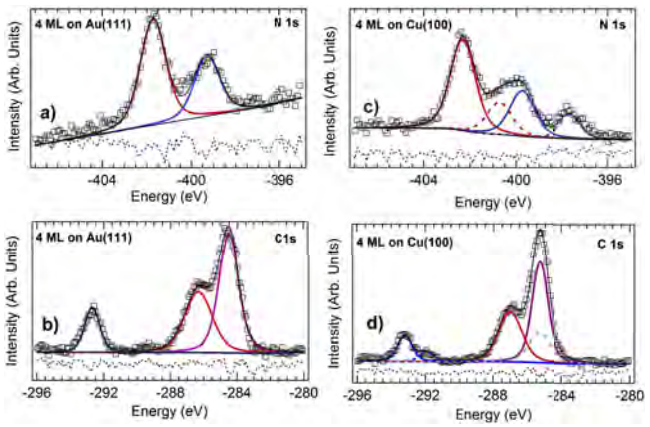

FIG. 7. N 1s and C 1s core level spectra for 4 ML thickness on the Au(111) ((a) and (b), respectively) and Cu(100) ((c) and (d), respectively) surfaces (open squares). Color coded spectral assignments are given in Fig. 4.

For the case of 4 ML of IL deposited on Cu(100), the evolution of the core levels presented in Fig. 6 is more complex. First, as a general trend, with the exception of C 1s, all core levels can be described by a linear combination of the core levels measured for 1 ML coverage with those measured for a multilayer. For example, the O 1s core level measured for 1 ML coverage is observed at −531.5 eV, whereas for the thicker layer, the main O 1s peak is found at −533.0 eV. It is clear that for a coverage of 2 ML, the O 1s peak is the sum, with nearly equal weight, of these two components. Upon further deposition of additional IL to the Cu(100) surface, the monolayer contribution to the O 1s core level is preserved while the higher binding energy multilayer O 1s contribution simply increases with film thickness. This can be generalized to other core levels: two pairs of N 1s and S 2p peaks are necessary to fit the N 1s and S 2p core levels, respectively, while two components are necessary to properly describe the F 1s core level evolution. This is illustrated in Fig. 7(c), where the N 1s core level can be fitted using two peaks corresponding to monolayer (dashed lines) and to multilayer (continuous lines) contributions. In this fit, the ratio monolayer/multilayer is fixed to 0.35. For the C 1s core level spectra, the latter spectral model is not applicable. For the thicker IL film on Cu(100), the C 1s spectrum shows the expected three components corresponding to the C–F bonds of the anion, the imidazolium and the alkyl chain of the cation, in decreasing order of binding energy. However, for 1 ML coverage, only two C 1s components are measured at −292.1 eV and −285.3 eV. This has been observed previously for a similar class of ionic liquids adsorbed on Ni(111), and has been attributed to a strong imidazolium ring interaction with the surface.[24] Indeed, a stronger imidazolium-Cu interaction can lead to a shorter ring-Cu distance, and thus to a much larger screening of the core holes during the photoemission process. Therefore, the C 1s contribution related to the imidazolium ring is shifted to lower binding energy, and overlaps with the C 1s contribution of the alkyl tail (as shown as a dashed gray line). The remaining core levels measured for a 4 ML film of IL are given in Fig. S5 of the supplementary material.

Some general aspects of the IL reactivity with the two surfaces can be drawn from the photoemission data. The behavior of the IL on Au(111) was studied previously where it was proposed that the IL anions and cations are both found in the first monolayer and interact with the surface without decomposition. These experiments were discussed as being consistent with a geometry such that the imidazolium ring is parallel to the surface with the alkyl tail directed into the vacuum and with the fluorinated part of the anion directed away from the surface as shown in Fig. S6 of the supplementary material.[23] Some of this information can be obtained by comparing the film compositions measured for multilayer and monolayer coverages; these are reported in Table S2 of the supplementary material. While a thick film of the IL displays a composition very close to the nominal composition of the IL, an ultrathin film coverage of 1 ML on Au(111) shows a rather different composition. In particular, the relative contributions from the cationic alkyl tail C 1s and the anionic F 1s intensities are increased, while the C 1s and N 1s contributions from the imidazolium ring are decreased. Using the UPS data from Fig. 5, we can refine the nature of the interface electronic structure as the small WF change measured after exposing the Au(111) surface to 1 ML of IL indicates that the IL adsorption leads to only a minor interface dipole, which results from a very small degree of charge transfer between the IL and the Au(111) surface. Thus $Im^{+}_{1,8}/NTf^{-}_{2}$ on Au(111) is a case of weak surface interaction.

The composition of 1 ML of IL on Cu(100) reported in the supplementary material, Table S2, indicates similar, if not stronger, trends in atomic composition, relative to those observed for Au(111). These could correspond to a comparable adsorption geometry on Cu(100), but with exacerbated features that result from a higher degree of structural order, itself a consequence of the stronger IL-Cu(100) interaction. These ideas are consistent with the UPS measurements of Fig. 5 featuring a large WF change upon deposition of 1 ML of the IL, due to a more significant charge rearrangement at the interface (charge transfer, pillow effect) and therefore to a stronger IL-surface interaction. This observation is also compatible with the STM results shown in Fig. 2, which indicate that little motion of the adsorbates occurs at room temperature on Cu(100). Fig. 6 also illustrates the stability of the first IL monolayer on Cu(100) through the persistence of the characteristic lower binding energy contribution to the photoemission spectra, even for higher IL coverages.

On the Au(111) surface, it is observed that core levels and VB peaks shift by about 0.2 eV for each additional deposition of IL. Such a shift to higher binding energies has often been interpreted as reduced screening of the core holes created further away from the metallic surface with increasing exposure.[23] Unexpectedly, very little broadening of the core levels was observed from 1 ML to higher coverages on the Au(111) surface, which is inconsistent with the latter picture. However, here we can see that the photoemission features follow the trend measured for the vacuum level. Therefore, the photoemission peak shifts could be a result of the IL energy levels alignment shift with respect to the Au substrate as a function of coverage. Similarly, after deposition of 1 ML on Cu(100), both VB and core level features follow the trend measured for the vacuum level: above 1 ML coverage all photoemission features are measured at a fixed binding energy. A schematic energy alignment diagram for the two surfaces upon increasing coverage is presented in Fig. 8. The Fermi level (FL) and the evolution of the energy alignment of the vacuum level (VL) as well as of one example of core level (O 1s) are presented as a function of the coverage on the two surfaces. The vacuum level shifts associated with interfacial dipoles are indicated in red. We note that for continuous and sufficiently thick films, the WF of the IL films should be relatively independent of the nature of the substrate metal (neglecting molecular orientation effects). This is indeed observed for our thick IL films, for which a WF of ~4 eV is measured. At the monolayer level, the O 1s spectrum measured on the Cu(100) surface has a much lower binding energy than expected for a rigid shift of the IL electronic structure with respect to the Cu(100) band structure. The reduced binding energy could be the result of a stronger screening of the core hole for the first monolayer on the Cu(100) surface.

The difference in WF evolution between the IL on Au(111) vs. on Cu(100) could have multiple origins. For the Au(111), a similar behavior at room temperature was observed for a

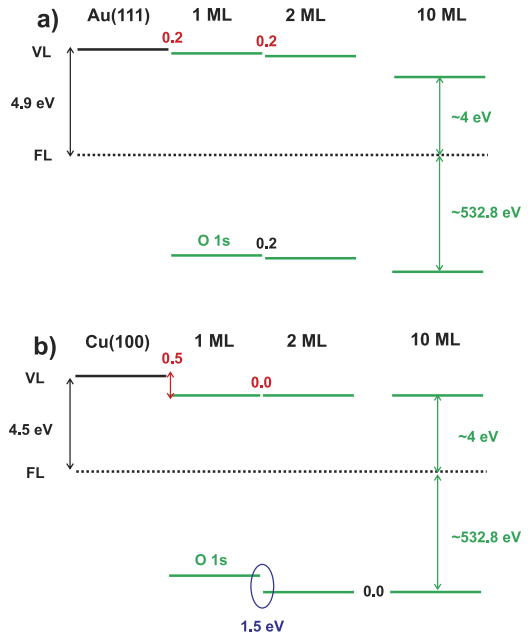

FIG. 8. Schematic energy diagram representing the vacuum level (VL), the Fermi level, and a typical core level, O 1s, positions as a function of the IL layer thickness on the (a) Au(111) and (b) Cu(100) surfaces. Work function changes are indicated in red.

related IL, $Im^{+}_{8,1}/BF^{-}_{4}$, but on Cu(111).[27] This was explained as resulting from incomplete layer-by-layer growth, with coexistence of island growth on top of film coverage. In our case, it is most likely that the amount of 3D growth would be small, given previous angle resolved photoemission work,[23] but precise angle resolved XPS measurements would be necessary to determine its contribution. Moreover, on Au(111), since the first layer does not appear to be strongly bound, it is possible that the entire film reorganizes upon deposition of additional molecules, therefore altering the resulting WF.

Finally, alternative adsorption modes have been proposed by Cremer *et al.* for similar ILs on Ni(111).[24] On Ni(111) it is believed that the $Im^{+}_{1,1}/NTf^{-}_{2}$ IL, akin to our IL but without a cationic alkyl tail, grows in a bilayer mode, where the anion is found above the imidazolium ring. We do not expect that this growth mode is possible in our case for Cu(100). Indeed, full coverage for this adsorption mode corresponds to a coverage twice the layer by layer coverage, and is incompatible with our coverage estimates for $Im^{+}_{1,8}/NTf^{-}_{2}$ on Cu(100) obtained from XPS analysis.

D. Top-down approach for monolayer formation

When the $Im^{+}_{8,1}/NTf^{-}_{2}$ IL is deposited on Au(111) or on Cu(100) at room temperature, no chemical decomposition of either the IL anions or cations was observed. A typical and useful technique to obtain monolayer coverage of organics on surfaces (and in particular on noble metal surfaces) is the so-called top-down approach, where a multilayer is annealed at a temperature large enough to desorb weakly bound molecules, leaving a residual monolayer. This is of course achievable only when the desorption temperature does not induce additional molecular chemistry at the surface of the metal. In the case of $Im^{+}_{1,8}/NTf^{-}_{2}$, annealing was performed at 130 °C, a temperature much lower than the molecular decomposition temperature, which was reported to be 230 °C for $Im^{+}_{1,8}/NTf^{-}_{2}$ from thermogravimetric analysis.[53]

Fig. 9 shows the core level spectra for 1 ML of $Im^{+}_{1,8}/NTf^{-}_{2}$ (red) and a multilayer annealed at 130 °C (black) on Au(111)

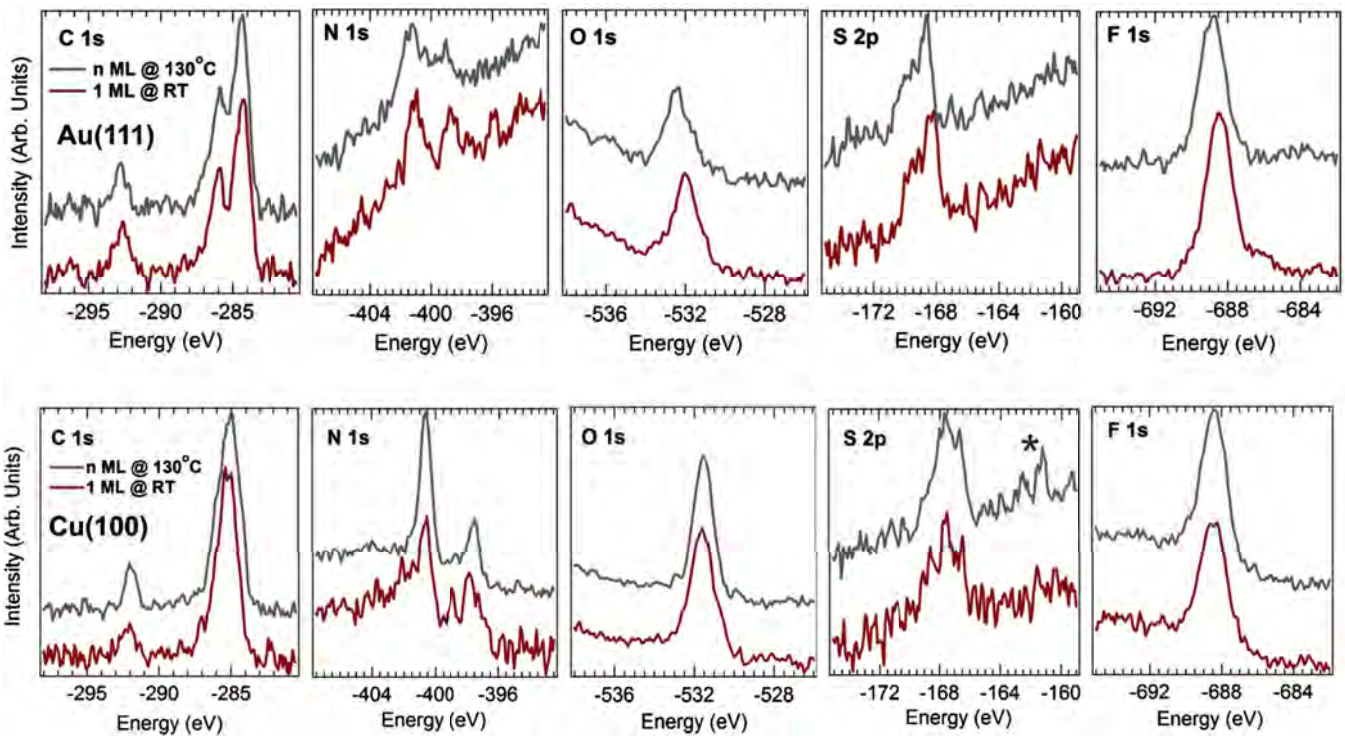

FIG. 9. Comparison of the C 1s, N 1s, O 1s, S 2p, and F 1s XPS core levels, measured for a 1 ML coverage deposited at room temperature and on a multilayer annealed to 130 °C for 10 min on Au(111) (top) and Cu(100) (bottom).

(top) and Cu(100) (bottom). The IL coverage obtained after annealing was determined as the ratio of the IL-related photoemission peaks to the metal (either Au or Cu) photoemission peaks. As shown in Fig. 9, the XPS data for 1 ML of $Im^+_{1,8}/NTf^-_2$ are nearly identical to that obtained from the annealing process at 130 °C. Moreover, the chemical species on each surface are identical to the one measured on 1 ML. This is particularly visible on the Cu(100) surface for the C 1s core level spectra of Fig. 9, which display only two peaks corresponding to the anion and the merged cations contributions. Thus, both the anion and cation appear to be quite stable on both Au(111) and Cu(100) surfaces at 130 °C. Only the S 2p peak at −160.6 eV, marked by an asterisk in Fig. 9, might indicate the presence of a small quantity of S–Cu bonds at the surface,[54–58] but the intensity of this contribution is close to our noise level and should be interpreted with caution.

Decomposition of the NTf^-_2 anion has been reported on Cu(111) surfaces at room temperature for sub-monolayers of a related IL, 1-butyl-1-methylpyrrolidinium/NTf^-_2.[38] However, XPS analysis of the C 1s core levels of the pyrrolidinium-based cation indicates a rather weak interaction with Cu, that could translate into high mobility of the cation at the surface of Cu(111). We therefore assume that the stability of NTf^-_2 is enhanced by the high degree of order and stability of the imidazolium-derived cation bond to Cu(100): at 1 ML coverage, NTf^-_2 could be prevented to reach a preferred Cu site leading to decomposition, or could be restricted to a conformation preventing reaction with Cu, due to the stabilizing presence of the imidazolium-based cations. Imidazole has a well known history of being used as a copper corrosion inhibitor.[59] Studies with *ex situ* preparation of imidazolium-containing films on copper surfaces all point to the formation of complex protective films.[60–65] A study of imidazolium halide ILs in an aqueous system also indicated that the presence of imidazolium inhibited electrochemical corrosion of copper.[66] This observation could be extended to trying other imidazolium-anion pairs to check for anion stabilization at the surface of copper, by the strong imidazolium-Cu bond.

IV. CONCLUSIONS

We have performed a comparative study of the adsorption of $Im^+_{8,1}/NTf^-_2$ on Au(111) and Cu(100) surfaces, using a combination of STM, UPS, and XPS spectroscopies. In particular, we have created ultrathin films ranging from 1 to 10 MLs by sequentially exposing the two surfaces to increasing doses of the IL in UHV. Core levels are characterized by XPS, while valence levels and the work function are characterized by UPS. Independently, STM images were measured before and after deposition of 1 ML of $Im^+_{1,8}/NTf^-_2$.

It is found that the chemical interaction of $Im^+_{1,8}/NTf^-_2$ on the Cu(100) surface is much stronger than on the Au(111) surface, leading to a very stable interfacial layer. The presence of this interfacial layer induces a strong charge rearrangement at the surface of Cu(100), with the creation of a large interface dipole. The adsorption geometry of the IL at 1 ML coverage is believed to be comparable to the one obtained on Au(111), where the two ions are found in equal number at the surface, presumably in a configuration that would minimize repulsion between like charges, with the imidazolium ring parallel to the surface, the alkyl tail pointing up, and the sulfonyl oxygens on the anions pointing downwards towards the metal surface, as illustrated in Fig. S6 of the supplementary material. This adsorption geometry is deduced both from atomic composition and from surface coverage estimation. Beyond monolayer coverage, while the experimental signature of the monolayer adsorbed on the Cu(100) surface remains visible and coexists with multilayer features, this is not observed on the Au(111) surface. The experimental results on Au(111) could indicate a large scale film reorganization upon deposition of additional layers, with loss of the monolayer conformation.

Additionally, we have shown that a monolayer coverage of the IL can be obtained on both Au(111) and Cu(100) via desorption of a multilayer at 130 °C, and that this monolayer presents signatures in photoemission that are nearly identical to the one measured for a single monolayer via direct deposition.

Finally, we propose that the strong imidazolium-Cu interaction may be inhibiting the decomposition of NTf^-_2 anion that was previously reported for NTf^-_2 paired with a non-planar, non-aromatic dialkylpyrrolidinium cation at room temperature. Additional studies should explore whether imidazolium-based cations could be an ideal choice to prevent the decomposition of other anions on Cu(100) as well.

SUPPLEMENTARY MATERIAL

See supplementary material for details on DOS calculations, photoemission cross section effects, details on the core levels pertaining to the IL and corresponding fit parameters, and schematic of the ion pair orientation on the surfaces.

ACKNOWLEDGMENTS

We gratefully acknowledge funding from NSF Grant No. CHE-1362272 to E.W.C. A.B.B. was previously supported by National Science Foundation Grant No. 0903661: Nanotechnology for Clean Energy IGERT.

[1] M. Armand, F. Endres, D. R. MacFarlane, H. Ohno, and B. Scrosati, "Ionic-liquid materials for the electrochemical challenges of the future," Nat. Mater. **8**, 621–629 (2009).
[2] E. D. Bates, R. D. Mayton, I. Ntai, and J. H. Davis, Jr., "CO_2 capture by a task-specific ionic liquid," J. Am. Chem. Soc. **124**, 926–927 (2002).
[3] R. Hayes, G. G. Warr, and R. Atkin, "Structure and nanostructure in ionic liquids," Chem. Rev. **115**, 6357–6426 (2015).
[4] F. Endres, O. Hofft, N. Borisenko, L. H. Gasparotto, A. Prowald, R. Al-Salman, T. Carstens, R. Atkin, A. Bund, and S. Z. El Abedin, "Do solvation layers of ionic liquids influence electrochemical reactions?," Phys. Chem. Chem. Phys. **12**, 1724–1732 (2010).
[5] F. Endres, N. Borisenko, S. Z. El Abedin, R. Hayes, and R. Atkin, "The interface ionic liquid(s)/electrode(s): *In situ* STM and AFM measurements," Faraday Discuss. **154**, 221–233 (2012).
[6] C. S. Santos and S. Baldelli, "Gas-liquid interface of room-temperature ionic liquids," Chem. Soc. Rev. **39**, 2136–2145 (2010).
[7] G. Law, P. R. Watson, A. J. Carmichael, and K. R. Seddon, "Molecular composition and orientation at the surface of room-temperature ionic liquids: Effect of molecular structure," Phys. Chem. Chem. Phys. **3**, 2879–2885 (2001).

[8]A. J. Carmichael, C. Hardacre, J. D. Holbrey, M. Nieuwenhuyzen, and K. R. Seddon, "Molecular layering and local order in thin films of 1-alkyl-3-methylimidazolium ionic liquids using X-ray reflectivity," Mol. Phys. **99**, 795–800 (2001).

[9]J. Bowers, M. C. Vergara-Gutierrez, and J. R. P. Webster, "Surface ordering of amphiphilic ionic liquids," Langmuir **20**, 309–312 (2004).

[10]T. Iimori, T. Iwahashi, H. Ishii, K. Seki, Y. Ouchi, R. Ozawa, H.-O. Hamaguchi, and D. Kim, "Orientational ordering of alkyl chain at the air/liquid interface of ionic liquids studied by sum frequency vibrational spectroscopy," Chem. Phys. Lett. **389**, 321–326 (2004).

[11]S. Rivera-Rubero and S. Baldelli, "Surface characterization of 1-butyl-3-methylimidazolium Br^-, I^-, PF_6^-, BF_4^-, $(CF_3SO_2)_2N^-$, SCN^-, $CH_3SO_3^-$, $CH_3SO_4^-$, and $(CN)_2N^-$ ionic liquids by sum frequency generation," J. Phys. Chem. B **110**, 4756–4765 (2006).

[12]Y. Jeon, J. Sung, W. Bu, D. Vaknin, Y. Ouchi, and D. Kim, "Interfacial restructuring of ionic liquids determined by sum-frequency generation spectroscopy and x-ray reflectivity," J. Phys. Chem. C **112**, 19649–19654 (2008).

[13]C. Ridings, V. Lockett, and G. Andersson, "Effect of the aliphatic chain length on electrical double layer formation at the liquid/vacuum interface in the $[C_n\text{mim}][BF_4]$ ionic liquid series," Phys. Chem. Chem. Phys. **13**, 17177–17184 (2011).

[14]T. Hammer, M. Reichelt, and H. Morgner, "Influence of the aliphatic chain length of imidazolium based ionic liquids on the surface structure," Phys. Chem. Chem. Phys. **12**, 11070–11080 (2010).

[15]K. R. J. Lovelock, "Influence of the ionic liquid/gas surface on ionic liquid chemistry," Phys. Chem. Chem. Phys. **14**, 5071–5089 (2012).

[16]I. J. Villar-Garcia, S. Fearn, G. F. De Gregorio, N. L. Ismail, F. J. V. Gschwend, A. J. S. McIntosh, and K. R. J. Lovelock, "The ionic liquid-vacuum outer atomic surface: A low-energy ion scattering study," Chem. Sci. **5**, 4404–4418 (2014).

[17]M. A. Tesa-Serrate, B. C. Marshall, J. E. J. Smoll, S. M. Purcell, M. L. Costen, J. M. Slattery, T. K. Minton, and K. G. McKendrick, "Ionic liquid-vacuum interfaces probed by reactive atom scattering: Influence of alkyl chain length and anion volume," J. Phys. Chem. C **119**, 5491–5505 (2015).

[18]K. Nakajima, S. Nakanishi, M. Lisal, and K. Kimura, "Surface structure of imidazolium-based ionic liquids: Quantitative comparison between simulations and high-resolution RBS measurements," J. Chem. Phys. **144**, 114702 (2016).

[19]S. Bovio, A. Podest, C. Lenardi, and P. Milani, "Evidence of extended solid-like layering in [Bmim][NTf2] ionic liquid thin films at room-temperature," J. Phys. Chem. B **113**, 6600–6603 (2009).

[20]F. Maier, T. Cremer, C. Kolbeck, K. R. J. Lovelock, N. Paape, P. S. Schulz, P. Wasserscheid, and H.-P. Steinrück, "Insights into the surface composition and enrichment effects of ionic liquids and ionic liquid mixtures," Phys. Chem. Chem. Phys. **12**, 1905–1915 (2010).

[21]T. Cremer, C. Kolbeck, K. R. J. Lovelock, N. Paape, R. Wölfel, P. S. Schulz, P. Wasserscheid, H. Weber, J. Thar, B. Kirchner, F. Maier, and H.-P. Steinrück, "Towards a molecular understanding of cation-anion interactions-probing the electronic structure of imidazolium ionic liquids by NMR spectroscopy, x-ray photoelectron spectroscopy and theoretical calculations," Chem. - Eur. J. **16**, 9018–9033 (2010).

[22]I. J. Villar-Garcia, E. F. Smith, A. W. Taylor, F. Qiu, K. R. J. Lovelock, R. G. Jones, and P. Licence, "Charging of ionic liquid surfaces under x-ray irradiation: The measurement of absolute binding energies by XPS," Phys. Chem. Chem. Phys. **13**, 2797–2808 (2011).

[23]T. Cremer, M. Stark, A. Deyko, H.-P. Steinrück, and F. Maier, "Liquid/solid interface of ultrathin ionic liquid films: $[C_1C_1\text{Im}][Tf_2N]$ and $[C_8C_1\text{Im}][Tf_2N]$ on Au(111)," Langmuir **27**, 3662–3671 (2011).

[24]T. Cremer, L. Wibmer, S. K. Calderon, A. Deyko, F. Maier, and H.-P. Steinrück, "Interfaces of ionic liquids and transition metal surfaces-adsorption, growth, and thermal reactions of ultrathin $[C_1C_1\text{Im}][Tf_2N]$ films on metallic and oxidised Ni(111) surfaces," Phys. Chem. Chem. Phys. **14**, 5153–5163 (2012).

[25]F. Rietzler, M. Piermaier, A. Deyko, H.-P. Steinrück, and F. Maier, "Electrospray ionization deposition of ultrathin ionic liquid films: $[C_8C_1\text{Im}]Cl$ and $[C_8C_1\text{Im}][Tf_2N]$ on Au(111)," Langmuir **30**, 1063–1071 (2014).

[26]M. Olschewski, R. Gustus, M. Marschewski, O. Hofft, and F. Endres, "Spectroscopic characterization of the interaction of lithium with thin films of the ionic liquid 1-octyl-3-methylimidazolium bis(trifluoromethylsulfonyl)amide," Phys. Chem. Chem. Phys. **16**, 25969–25977 (2014).

[27]K. L. Syres and R. G. Jones, "Adsorption, desorption, and reaction of 1-octyl-3-methylimidazolium tetrafluoroborate, $[C_8C_1\text{Im}][BF_4]$, ionic liquid multilayers on Cu(111)," Langmuir **31**, 9799–9808 (2015).

[28]D. Yoshimura, T. Yokoyama, T. Nishi, H. Ishii, R. Ozawa, H.-O. Hamaguchi, and K. Seki, "Electronic structure of ionic liquids at the surface studied by UV photoemission," J. Electron Spectrosc. Relat. Phenom. **144–147**, 319–322 (2005).

[29]T. Iwahashi, T. Nishi, H. Yamane, T. Miyamae, K. Kanai, K. Seki, D. Kim, and Y. Ouchi, "Surface structural study on ionic liquids using metastable atom electron spectroscopy," J. Phys. Chem. C **113**, 19237–19243 (2009).

[30]K. Kanai, T. Nishi, T. Iwahashi, Y. Ouchi, K. Seki, Y. Harada, and S. Shin, "Electronic structures of imidazolium-based ionic liquids," J. Electron Spectrosc. Relat. Phenom. **174**, 110–115 (2009).

[31]M. Reinmöller, A. Ulbrich, T. Ikari, J. Preiss, O. Höfft, F. Endres, S. Krischok, and W. J. D. Beenken, "Theoretical reconstruction and elementwise analysis of photoelectron spectra for imidazolium-based ionic liquids," Phys. Chem. Chem. Phys. **12**, 19526–19533 (2011).

[32]A. Ulbrich, M. Reinmöller, W. J. D. Beenken, and S. Krischok, "Surface electronic structure of [XMIm]Cl probed by surface-sensitive spectroscopy," ChemPhysChem **13**, 1718–1724 (2012).

[33]S. Krischok, A. Ulbrich, T. Ikari, V. Kempter, M. Marschewski, and O. Höfft, "Surface structure of $[\text{XMIm}]Tf_2N$ ultrathin ionic liquid films probed by metastable He atoms and photoelectron spectroscopies (UPS and XPS)," Nucl. Instrum. Methods Phys. Res., Sect. B **340**, 51–57 (2014).

[34]R. Foulston, S. Gangopadhyay, C. Chiutu, P. Moriarty, and R. G. Jones, "Mono- and multi-layer adsorption of an ionic liquid on Au(110)," Phys. Chem. Chem. Phys. **14**, 6054–6066 (2012).

[35]A. Ulbrich, M. Reinmller, W. J. Beenken, and S. Krischok, "Photoelectron spectroscopy on ionic liquid surfaces—Theory and experiment," J. Mol. Liq. **192**, 77–86 (2014).

[36]E. M. McIntosh, J. Ellis, A. P. Jardine, P. Licence, R. G. Jones, and W. Allison, "Probing liquid behaviour by helium atom scattering: Surface structure and phase transitions of an ionic liquid on Au(111)," Chem. Sci. **5**, 667–676 (2014).

[37]T. Waldmann, H.-H. Huang, H. E. Hoster, O. Höfft, F. Endres, and R. J. Behm, "Imaging an ionic liquid adlayer by scanning tunneling microscopy at the solid—Vacuum interface," ChemPhysChem **12**, 2565–2567 (2011).

[38]B. Uhl, F. Buchner, S. Gabler, M. Bozorgchenani, and R. J. Behm, "Adsorption and reaction of sub-monolayer films of an ionic liquid on Cu(111)," Chem. Commun. **50**, 8601–8604 (2014).

[39]B. Uhl, H. Huang, D. Alwast, F. Buchner, and R. J. Behm, "Interaction of ionic liquids with noble metal surfaces: Structure formation and stability of [OMIM][TFSA] and [EMIM][TFSA] on Au(111) and Ag(111)," Phys. Chem. Chem. Phys. **17**, 23816–23832 (2015).

[40]R. Wen, B. Rahn, and O. M. Magnussen, "Potential-dependent adlayer structure and dynamics at the ionic Liquid/Au(111) interface: A molecular-scale *in situ* video-STM study," Angew. Chem., Int. Ed. **54**, 6062–6066 (2015).

[41]T. Cremer, M. Killian, J. M. Gottfried, N. Paape, P. Wasserscheid, F. Maier, and H.-P. Steinrueck, "Physical vapor deposition of $[\text{EMIM}][Tf_2N]$: A new approach to the modification of surface properties with ultrathin ionic liquid films," ChemPhysChem **9**, 2185–2190 (2008).

[42]A. Keppler, M. Himmerlich, T. Ikari, M. Marschewski, E. Pachomow, O. Höfft, W. Maus-Friedrichs, F. Endres, and S. Krischok, "Changes of the near-surface chemical composition of the 1-ethyl-3-methylimidazolium bis(trifluoromethylsulfonyl)imide room temperature ionic liquid under the influence of irradiation," Phys. Chem. Chem. Phys. **13**, 1174–1181 (2011).

[43]M. S. Gordon and M. W. Schmidt, *Theory and Applications of Computational Chemistry: The First Forty Years*, Advances in Electronic Structure Theory: GAMESS a Decade Later (Elsevier, Amsterdam, 2005), pp. 1167–1189.

[44]I. Horcas, R. Fernandez, J. M. Gomez-Rodriguez, J. Colchero, J. Gomez-Herrero, and A. M. Baro, "WSXM: A software for scanning probe microscopy and a tool for nanotechnology," Rev. Sci. Instrum. **78**, 013705 (2007).

[45]J. P. Leal, J. M. S. S. Esperança, M. E. M. da Piedade, J. N. C. Lopes, L. P. N. Rebelo, and K. R. Seddon, "The nature of ionic liquids in the gas phase," J. Phys. Chem. A **111**, 6176–6182 (2007).

[46]M. S. Kelkar and E. J. Maginn, "Calculating the enthalpy of vaporization for ionic liquid clusters," J. Phys. Chem. B **111**, 9424–9427 (2007).

[47]D. Strasser, F. Goulay, M. S. Kelkar, E. J. Maginn, and S. R. Leone, "Photoelectron spectrum of isolated ion-pairs in ionic liquid vapor," J. Phys. Chem. A **111**, 3191–3195 (2007).

[48]J. P. Armstrong, C. Hurst, R. G. Jones, P. Licence, K. R. J. Lovelock, C. J. Satterley, and I. J. Villar-Garcia, "Vapourisation of ionic liquids," Phys. Chem. Chem. Phys. **9**, 982–990 (2007).
[49]J. H. Gross, "Molecular ions of ionic liquids in the gas phase," J. Am. Soc. Mass Spectrom. **19**, 1347–1352 (2008).
[50]C. J. Powell and A. Jablonski, NIST Electron Effective-Attenuation-Length Database - Version 1.3, National Institute of Standards and Technology, 2011.
[51]H. B. Michaelson, "The work function of the elements and its periodicity," J. Appl. Phys. **48**, 4729 (1977).
[52]P. O. Gartland, S. Berge, and B. J. Slagsvold, "Photoelectric work function of a copper single crystal for the (100), (110), (111), and (112) faces," Phys. Rev. Lett. **28**, 738–739 (1972).
[53]H. Luo, G. A. Baker, and S. Dai, "Isothermogravimetric determination of the enthalpies of vaporization of 1-alkyl-3-methylimidazolium ionic liquids," J. Phys. Chem. B **112**, 10077 (2008).
[54]Y. Ma, P. Rudolf, E. E. Chaban, C. T. Chen, G. Meigs, and F. Sette, "Multiple sulfur sites in the Cu(100) p(2×2)–S surface structure," Phys. Rev. B **41**, 5424–5427 (1990).
[55]M. Polcik, L. Wilde, J. Haase, B. Brena, D. Cocco, G. Comelli, and G. Paolucci, "Adsorption and temperature-dependent decomposition of SO_2 on Cu(100) and Cu(111): A fast and high-resolution core-level spectroscopy study," Phys. Rev. B **53**, 13720–13724 (1996).
[56]H. Lu, E. Janin, M. Dvila, C. Pradier, and M. Gthelid, "Adsorption of SO_2 on Cu(100) and Cu(100)–c(2×2)–O surfaces studied with photoelectron spectroscopy," Vacuum **49**, 171–174 (1998).
[57]A. R. Alemozafar, X.-C. Guo, and R. J. Madix, "Adsorption and reaction of sulfur dioxide with Cu(110) and Cu(110)–p(21)–O," J. Chem. Phys. **116**, 4698–4706 (2002).
[58]J. Jia, A. Bendounan, K. Chaouchi, and V. A. Esaulov, "Sulfur interaction with Cu(100) and Cu(111) surfaces: A photoemission study," J. Phys. Chem. C **118**, 24583–24590 (2014).
[59]M. Antonijevic and M. Petrovic, "Copper corrosion inhibitors. A review," Int. J. Electrochem. Sci. **3**, 1–28 (2008).
[60]J. E. J. Bauman and J. C. Wang, "Imidazole complexes of nickel(II), copper(II), zinc(II), and silver(I)," Inorg. Chem. **3**, 368–373 (1964).
[61]S. Yoshida and H. Ishida, "A study on the orientation of imidazoles on copper as corrosion inhibitor and possible adhesion promoter for electric devices," J. Chem. Phys. **78**, 6960–6969 (1983).
[62]G. Xue, S. Jiang, X. Huang, G. Shi, and B. Sun, "Chemical reaction of metallic copper with imidazole," J. Chem. Soc., Dalton Trans. 1487–1488 (1988).
[63]R. Gašparac, C. R. Martin, and E. Stupnišek-Lisac, "*In situ* studies of imidazole and its derivatives as copper corrosion inhibitors. I. Activation energies and thermodynamics of adsorption," J. Electrochem. Soc. **147**, 548–551 (2000).
[64]R. Gašparac, C. R. Martin, E. Stupnišek-Lisac, and Z. Mandic, "*In situ* and *ex situ* studies of imidazole and its derivatives as copper corrosion inhibitors. II. AC impedance, XPS, and SIMS studies," J. Electrochem. Soc. **147**, 991–998 (2000).
[65]B. H. Loo, Y. Tse, K. Parsons, C. Adelman, A. El-Hage, and Y. G. Lee, "Surface-enhanced Raman spectroscopy of imidazole adsorbed on electrode and colloidal surfaces of Cu, Ag, and Au," J. Raman Spectrosc. **37**, 299–304 (2006).
[66]M. Scendo and J. Uznanska, "The effect of ionic liquids on the corrosion inhibition of copper in acidic chloride solutions," Int. J. Corros. **2011**, 718626 (2011).